Supplementary material: calculating decompression rates from vesicle number densities

In pumice, nucleation is inferred to be continuous throughout ascent (e.g. Blower et al., 2001; Klug et al., 2002; Gurioli et al., 2005; Shea et al., 2010b); hence the total number of vesicles measured will reflect an accumulation of nucleation time-intervals. To avoid using the total N_V, which integrates the number density over the entire decompression path, we utilize only number densities calculated for the size range 0.01-0.001 mm to capture the decompression rates corresponding to the final stages of rapid ascent prior to fragmentation (labeled N_{Vf} to denote their correspondence to only the final accelerating portions of the ascent path). All vesicle number densities are normalized to melt volume to account for gas expansion (N_{Vf}^{corr} ,Table DR1 in the data repository).

As mentioned in the main text, we use equations presented in Toramaru (1995, 2006) to derive *dP*/*dt* from number density:

$$N_{V\,calc} = 34 X_0 \alpha_1^{-2} \alpha_2^{-\frac{1}{4}} \alpha_3^{-\frac{3}{2}}, \qquad (1)$$

where X_0 is the initial water concentration at the saturation pressure chosen as 4.9 wt% and 3.5 wt% for the white and the gray magma respectively (Cioni et al., 1995, 1998; Cioni, 2000; Larsen, 2008; Shea et al., 2009, 2010b). α_1, α_2, α_3 represent dimensionless parameters (Toramaru, 1995) defined as:

$$\alpha_1 = \frac{16\pi\sigma_{HOM}^3}{3kTP_0^2}, \qquad (2)$$

$$\alpha_2 = \frac{\Omega_M P_0}{kT}, \qquad (3)$$

$$\alpha_3 = \frac{kTX_0DP_0}{4\sigma_{HOM}^2\left|\frac{dP}{dt}\right|}, \quad (4)$$

where k is the Boltzmann constant, Ω_M the volume of water molecules in the melt taken as 2.6×10^{-29} m^3, P_0 the initial pressure (calculated as a function of X_0 using solubility models), and T the temperature, set at 850˚C for EU1, 900˚C for EU2, 975˚C for EU2/3 (PC1), and 1050˚C for all other gray magma products (Cioni et al., 1995, 1998 and Shea et al., 2009). For similar magma compositions, the water diffusivity D depends primarily on temperature and dissolved water content in melt (e.g. Zhang and Behrens, 2000). Larsen (2008) and Shea et al. (2010b) used values of 2×10^{-12} for the 79AD white magma (i.e. EU1 and EU2). For the gray magma, we use values of 2×10^{-11} m^2 s^{-1} an order of magnitude higher, to account for the temperature difference and the lower initial H_2O contents (e.g. Watson, 1994). These diffusivity values assume water saturation at the initial pressure (X_0=4.9 wt% and 3.5 wt% for the white and gray magmas, respectively). However, the values of N_{Vf}^{corr} replaced with N_{Vcalc} in Eq. (1) to derive *dP/dt* only represent the small vesicle populations, and thereby the last stages of nucleation. Because a fraction of the initial water was used for vesiculation of earlier vesicle populations, the diffusivity values need to be modified to account for this. Thus, in all equations, the initial pressure and water contents need to be set at values corresponding to late-stage nucleation. Because we possess measurements of porosity for each vesicle size category (i.e. through FOAMS outputs), we can calculate the predicted water content at a given porosity by rearranging the equilibrium model presented in Gardner et al. (1999):

$$X_F = X_I - \frac{\phi}{\frac{\rho}{Z}\overline{V}_W(1-\phi)}, \quad (5)$$

where X_I and X_F are initial water content and final water content at porosity ϕ, Z is molecular weight of water, $\overline{V}_W$ is the molar volume of water in the vapor phase, and ρ the magma density. For each measured clast, we used the porosity value obtained by summing the contributions from all vesicles with sizes $L \geq 0.01$ mm to derive X_F. The latter value replaces X_0 in Equations (1) to

(4). New initial pressures P_0 were also calculated using X_F based on solubility models experimentally calibrated by Larsen (2008) for the white magma, and calculated from the macro H2OSOLvX1 by Moore (2008) for the gray magma. Typically, calculated water contents X_F were ~2 wt% lower than the initial pre-vesiculation values of 3.5 and 4.5 wt%. Hence, to mimic D vs. H_2O relationships measured in other magmas (e.g. Watson, 1994; Zhang and Behrens, 2000), diffusivity was lowered by a factor of ~5 to account for the lower water content.

Because nucleation is inferred to be heterogeneous in 79AD Vesuvius magmas (Larsen, 2008; Shea et al., 2010b), we replace σ_{HOM} in Eq. (1) by an "effective" surface tension σ_{EFF} that incorporates the activation energy reduction term φ, expressed as $\sigma_{EFF} = \varphi^{1/3}\sigma_{HOM}$ (Cluzel et al., 2008). Since bubble nucleation is strongly controlled by the presence of tiny oxide microlites, σ_{EFF} is set at 0.035 N m^{-1} for both the white and the gray magma, similar to values found by Mangan and Sisson (2005), as well as by Mourtada-Bonnefoi and Laporte (2004) for dacites, and by Shea et al. (2010b) for phonolites. Once all required parameters are calculated, curves of dP/dt vs. N_{Vcalc} were used to determine the decompression rate that best matched N_{Vcorr} measured in natural samples from both fall and PDC phases of the eruption. For layer EU2/3pf (transition from white to gray pumice), dP/dt was calculated using values of diffusivity and temperature intermediate between the white and gray magmas (Table DR1). Figure DR1 below shows an example of a dP/dt vs. N_{Vcalc} plot used to calibrate decompression rates for the white magma (from Shea et al., 2010b). In this case, values of number densities for EU1 and EU2 mean densities are shown as orange and blue arrays, and for surface tension values taken at 0.035 N m^{-1}, corresponding decompression rates are around 0.4 and 1.1 MPa s^{-1} respectively.

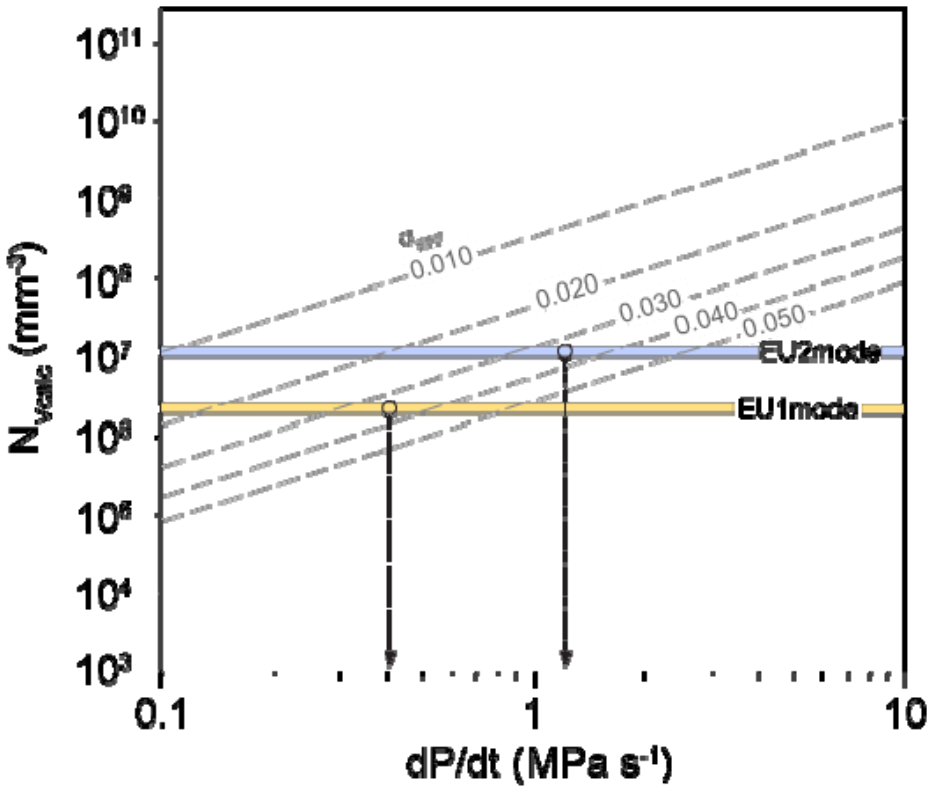

Figure DR1

Additional References not in the main text

Blower, J.D., Keating, J.P., Mader, H.M., Phillips, J.C., 2001, Inferring volcanic degassing processes from vesicle size distributions: Geophysical Research Letters, v. 28, p. 347–350. doi: 10.1029/2000GL012188.

Cioni, R., Civetta, L., Marianelli, P., Metrich, N., Santacroce, R., Sbrana, A., 1995, Compositional layering and syn-eruptive mixing of periodically refilled shallow magma chamber: the A.D. 79 Plinian eruption of Vesuvius: Journal Petrology, v. 36, p. 739–776.

Cioni, R., Marianelli, P., Santacroce, R., 1998, Thermal and compositional evolution of the shallow magma chamber of Vesuvius: Evidence from pyroxene phenocrysts and melt inclusions: Journal of Geophysical Research, v. 103, B8-18277, doi:10.1029/98JB01124.

Cioni, R., 2000, Volatile content and degassing processes in the 79AD magma chamber at Vesuvius (Italy): Contributions to Mineralogy and Petrology, v. 140, p. 40–54.

Cluzel, N., Laporte, D., Provost, A., Kannewischer, I., 2008, Kinetics of heterogeneous bubble nucleation in rhyolitic melts: implications for the number density of bubbles in volcanic conduits and for pumice textures: Contributions to Mineralogy and Petrology, v. 156, p. 745–763.

Gardner, J.E., Hilton, M., Carroll, M.R., 1999, Experimental constraints on degassing of magma: isothermal bubble growth during continuous decompression from high pressure: Earth Planetary Science Letters, v. 168, p. 201–218.

Klug, C., Cashman, K.V., Bacon, C., 2002, Structure and physical characteristics of pumice from the climactic eruption of Mount Mazama (Crater Lake), Oregon: Bulletin of Volcanology, v. 64, p. 486– 501.

Larsen, J.F., 2008, Heterogeneous bubble nucleation and disequilibrium H_2O exsolution in Vesuvius K-phonolite melts: Journal of Volcanology and Geothermal Research, v. 275, p. 278–288.

Mangan, M.T., Sisson, T.W., 2005, Evolution of melt-vapor surface tension in silicic volcanic systems: experiments with hydrous melts: Journal of Geophysical Research, v. 110, B01202, doi:10.1029/2004JB003215.

Moore, G., 2008, Interpreting H2O and CO2 contents in melt inclusions: constraints from solubility experiments and modeling: Reviews in Mineralogy, v. 69, p. 331–369.

Mourtada-Bonnefoi, C.C., Laporte, D., 2004, Kinetics of bubble nucleation in a rhyolitic melt: an experimental study of the effect of ascent rate: Earth and Planetary Science Letters, v. 218, p. 521–537.

Shea, T., Larsen, J.F., Gurioli, L., Hammer, J.E., Houghton, B.F., Cioni, R., 2009, Leucite crystals: surviving witnesses of magmatic processes preceding the 79AD eruption at Vesuvius, Italy: Earth and Planetary Science Letters, v. 281, p. 88–98. doi: 10.1016/j.epsl.2009.02.014.

Toramaru, A., 1995, Numerical study of nucleation and growth of bubbles in viscous magmas: Journal of Geophysical Research, v. 100, B02775, doi:10.1029/94JB02775.

Watson, E.B., 1994, Diffusion in volatile-bearing magmas: Reviews in Mineralogy, v. 30, p. 371–411.

Zhang, Y., Behrens, H., 2000, H2O diffusion in rhyolitic melts and glasses: Chemical Geology, v. 169, p. 243–262.

Table DR1: Main textural parameters of pumice from fall and PDCs

	Density	Φ [a] %	ρ [b] (g cm^{-3})	N_{vf}^{corr} [c] (mm^{-3})	dP/dt [d] (MPa s^{-1})	X_{corr} [e] %	Lc_{corr} [f] %	V_{gl} [g] %	Φ_{conn} [h]
Unit		%	g cm^{-1}	mm^{-3}	MPa s^{-1}	%	%	%	%
EU1 fall	low	81.4	0.48	(4.7) 2.8×10^{6}	0.38	6.1	22.0	11.5	
	modal	75	0.87	(3.3) 3.3×10^{6}	0.40	4.1	18.0	17.0	
	high	62.1	0.98	(8.3) 8.0×10^{6}	0.66	5.8	14.0	27.7	
EU2 fall	low	83.4	0.41	(13) 11.3×10^{6}	0.98	4.1	13.0	10.9	100%
	modal	77	0.60	(16) 15.2×10^{6}	1.13	6.1	14.0	15.6	93.6%
	high	70.9	0.76	(17) 16.0×10^{6}	1.15	5.4	17.5	20.5	90.5%
EU3 base	low	76.9	0.6	(7.9) 7.1×10^{6}	7.78	3.5	28.7	15.7	
	modal	64.5	0.92	(2.7) 2.4×10^{6}	3.17	6.2	21.2	25.8	
	high	50.1	1.3	(2.2) 2.0×10^{6}	2.35	6.0	19.3	37.3	
EU3 max	low	67.4	0.85	(7.0) 6.4×10^{6}	6.63	3.4	17.7	25.7	
	modal	59.6	1.05	(6.7) 6.4×10^{6}	6.20	3.7	20.8	30.5	
	high	52.2	1.24	(4.9) 4.7×10^{6}	4.65	3.6	35.1	29.7	
EU3 top	low	80	0.52	(13) 11.7×10^{6}	11.53	5.0	22.3	14.6	100%
	modal	72	0.72	(14) 12.2×10^{6}	11.07	9.0	34.6	15.8	100%
	high	55.7	1.16	(6.5) 6.2×10^{6}	5.83	4.3	35.9	26.5	100%
EU4 fall	low	82.8	0.45	(12) 10.4×10^{6}	11.10	7.0	40.7	9.0	
	modal	73.1	0.7	(9.7) 8.8×10^{6}	8.89	4.3	33.6	16.7	
	high	62.4	0.98	(7.4) 6.9×10^{6}	6.74	5.9	28.4	24.7	
P1	low	77.9	0.57	(5.7) 4.9×10^{6}	3.19 [i]	5.4	28.4	14.6	
	modal	70.8	0.76	(7.3) 6.8×10^{6}	3.77 [i]	4.8	15.9	23.2	
	high	67.9	0.83	(11) 10.6×10^{6}	5.01 [i]	5.3	21.1	23.6	
P2	low	83.7	0.42	(12) 10.3×10^{6}	10.95	8.0	17.5	12.1	
	modal	66.2	0.88	(4.3) 3.7×10^{6}	4.38	6.8	17.8	25.5	
	modal 2	60.6	1.02	(7.2) 6.5×10^{6}	6.29	4.1	27.0	27.2	
	low	52.6	1.23	(6.7) 6.2×10^{6}	5.70	7.2	32.8	28.4	
P3	low	74.1	0.67	(9.3) 8.4×10^{6}	8.45	5.0	18.4	19.9	
	modal	67.6	0.84	(7.0) 6.3×10^{6}	6.59	5.9	16.1	25.3	
	high	52.8	1.23	(8.8) 6.0×10^{6}	5.54	5.5	34.8	28.2	
P4	low	74	0.68	(11) 9.7×10^{6}	9.55	7.7	24.2	17.7	
	modal	67.9	0.83	(10) 8.7×10^{6}	8.08	7.2	32.3	19.4	
	high	51.9	1.25	(9.9) 9.7×10^{6}	7.72	4.8	25.0	33.8	
P5	low	82.4	0.46	(17) 12.7×10^{6}	12.75	8.5	35.6	9.8	100%
	modal	73.4	0.69	(9.1) 8.4×10^{6}	8.55	7.1	22.6	18.7	100%
	high	58.1	1.09	(5.0) 4.3×10^{6}	4.46	7.2	22.9	29.3	98.3%
P6	low	77.5	0.59	(5.3) 4.4×10^{6}	5.53	6.7	23.4	15.7	
	modal	33	1.74	(4.2) 0.4×10^{6}	0.60	5.5	42.8	34.6	
	high	62.1	0.99	(3.7) 2.2×10^{6}	2.84	5.3	27.2	25.6	

	Density	Φ [a]	ρ [b]	N_{vf}^{corr} [c]	dP/dt [d]	X_{corr} [e]	Lc_{corr} [f]	V_{gl} [g]	Φ_{conn} [h]
Unit		%	g cm^{-1}	mm^{-3}	MPa s^{-1}	%	%	%	%
EU1 fall	low	81.4	0.48	(4.7) 2.8×10^{6}	0.38	6.1	22.0	11.5	
	modal	75	0.87	(3.3) 3.3×10^{6}	0.40	4.1	18.0	17.0	
	high	62.1	0.98	(8.3) 8.0×10^{6}	0.66	5.8	14.0	27.7	
EU2 fall	low	83.4	0.41	(13) 11.3×10^{6}	0.98	4.1	13.0	10.9	100%
	modal	77	0.60	(16) 15.2×10^{6}	1.13	6.1	14.0	15.6	93.6%
	high	70.9	0.76	(17) 16.0×10^{6}	1.15	5.4	17.5	20.5	90.5%
EU3 base	low	76.9	0.6	(7.9) 7.1×10^{6}	7.78	3.5	28.7	15.7	
	modal	64.5	0.92	(2.7) 2.4×10^{6}	3.17	6.2	21.2	25.8	
	high	50.1	1.3	(2.2) 2.0×10^{6}	2.35	6.0	19.3	37.3	
EU3 max	low	67.4	0.85	(7.0) 6.4×10^{6}	6.63	3.4	17.7	25.7	
	modal	59.6	1.05	(6.7) 6.4×10^{6}	6.20	3.7	20.8	30.5	
	high	52.2	1.24	(4.9) 4.7×10^{6}	4.65	3.6	35.1	29.7	
EU3 top	low	80	0.52	(13) 11.7×10^{6}	11.53	5.0	22.3	14.6	100%
	modal	72	0.72	(14) 12.2×10^{6}	11.07	9.0	34.6	15.8	100%
	high	55.7	1.16	(6.5) 6.2×10^{6}	5.83	4.3	35.9	26.5	100%
EU4 fall	low	82.8	0.45	(12) 10.4×10^{6}	11.10	7.0	40.7	9.0	
	modal	73.1	0.7	(9.7) 8.8×10^{6}	8.89	4.3	33.6	16.7	
	high	62.4	0.98	(7.4) 6.9×10^{6}	6.74	5.9	28.4	24.7	
P1	low	77.9	0.57	(5.7) 4.9×10^{6}	3.19 [i]	5.4	28.4	14.6	
	modal	70.8	0.76	(7.3) 6.8×10^{6}	3.77 [i]	4.8	15.9	23.2	
	high	67.9	0.83	(11) 10.6×10^{6}	5.01 [i]	5.3	21.1	23.6	
P2	low	83.7	0.42	(12) 10.3×10^{6}	10.95	8.0	17.5	12.1	
	modal	66.2	0.88	(4.3) 3.7×10^{6}	4.38	6.8	17.8	25.5	
	modal 2	60.6	1.02	(7.2) 6.5×10^{6}	6.29	4.1	27.0	27.2	
	low	52.6	1.23	(6.7) 6.2×10^{6}	5.70	7.2	32.8	28.4	
P3	low	74.1	0.67	(9.3) 8.4×10^{6}	8.45	5.0	18.4	19.9	
	modal	67.6	0.84	(7.0) 6.3×10^{6}	6.59	5.9	16.1	25.3	
	high	52.8	1.23	(8.8) 6.0×10^{6}	5.54	5.5	34.8	28.2	
P4	low	74	0.68	(11) 9.7×10^{6}	9.55	7.7	24.2	17.7	
	modal	67.9	0.83	(10) 8.7×10^{6}	8.08	7.2	32.3	19.4	
	high	51.9	1.25	(9.9) 9.7×10^{6}	7.72	4.8	25.0	33.8	
P5	low	82.4	0.46	(17) 12.7×10^{6}	12.75	8.5	35.6	9.8	100%
	modal	73.4	0.69	(9.1) 8.4×10^{6}	8.55	7.1	22.6	18.7	100%
	high	58.1	1.09	(5.0) 4.3×10^{6}	4.46	7.2	22.9	29.3	98.3%
P6	low	77.5	0.59	(5.3) 4.4×10^{6}	5.53	6.7	23.4	15.7	
	modal	33	1.74	(4.2) 0.4×10^{6}	0.60	5.5	42.8	34.6	
	high	62.1	0.99	(3.7) 2.2×10^{6}	2.84	5.3	27.2	25.6	

Table DR2: Componentry of deposits from the magmatic phase of the A.D. 79 eruption

	EU1	EU2base	EU2max	EU2top	P1	P1	EU3base	EU3max	P2-4	P5	P6	EU4	EU4
Reference	B1989	B1989	L1973	B1989	G99-02	B1989	B1989	L1973	G99-02	G99-02	G99-02	G99-02	B1989
X_{JUV} [a] max					100%					83.4%	26.6%		
X_{JUV} mean	48.4%	84.1%	96.4%	92.7%	90.0%	86.9%	86.8%	90.9%	93.3%	80.1%	23.0%	62.8%	70.9%
X_{JUV} min					86.4%					76.8%	18.1%		
X_{WR} max					2.1%					18.1%	72.3%		
X_{WR} mean	49.0%	15.2%	3.1%	6.7%	1.6%	11.5%	12.4%	7.5%	3.6%	15.1%	67.3%	31.6%	28.0%
X_{WR} min					0%					12.8%	63.6%		
Wallrock Type [b]	l, lm, m, sk	l, lm, m,sk	l, lm, m	l, lm	l, lm	l, lm	l, lm, m	l, lm	l, lm, m	l, lm, m	l	l, lm, m, sk, c	“
X_{XTL} max					11.5%					5.0%	9.8%		
X_{XTL} mean	2.6%	0.7%	0.5%	0.6%	8.4%	1.6%	0.8%	1.6%	3.1%	4.8%	9.7%	5.6%	1.1%
X_{XTL} min					0%					3.7%	9.6%		

a. X_{JUV} X_{WR} X_{XTL}=Juvenile, wallrock and crystal content % volume respectively.
b. Wallrock types: l: lavas (density~2.4-2.6), lm: limestones (density ~2.7), m: marbles (density ~2.7), c: cumulites (density ~3.2), sk: metasomatic skarns (density ~3.0-3.2). Wallrock componentries were obtained using a 0.063-32 mm size range. Note: densities for the lithic material in g cm^{-3} within the parentheses are from Barberi et al. (1989) and references therein. Because wall-rocks entrained within PDCs can segregate at the base during transport, the values reported for PDCs are subject to more uncertainty than values measured in fall samples.

Reference abbreviations: B1989=Barberi et al. (1989) L1973=Lirer et al. (1973) G99-02=Gurioli et al. (1999, 2002)

Table DR3: Eruptive parameters measured/calculated for the magmatic phase of the eruption.

	White magma		Gray magma		References
Parameters	*EU1*	*EU2*	$EU3_{base\text{-}max}$ [i]	$EU3_{top}$	
ρ_{MAGMA} [a]	2520 kg m^{-3}	2550 kg m^{-3}	2625 kg m^{-3}	2625 kg m^{-3}	Shea et al. (in prep)
	840˚C	900-925˚C	1050˚C	1050˚C	Cioni et al. (1995, 1998, Shea et al. (2009)
$X_{crystals}$ [c]	23.3%	20%	28.3%	37%	Shea et al. (2009), This study
At P=100 MPa [d]					
μ_{m+c}	3.4×10^3 Pa s	1.5×10^3	2.4×10^2	8.6×10^2	Shaw (1972)
μ_{m+c+b} [1]	3.0×10^3	1.0×10^3	4.0×10^2	8.0×10^2	Lejeune and Richet (1995)
μ_{m+c+b} [2]	4.0×10^3	2.0×10^3	4.2×10^2	9.0×10^2	Mangan et al. (1998)
At P=15 MPa [d]					
μ_{m+c}	1.3×10^5	3.2×10^4	4.2×10^3	7.9×10^3	
μ_{m+c+b} [1]	3.0×10^4	8.0×10^3	1.0×10^3	3.0×10^3	
μ_{m+c+b} [2]	5.0×10^5	1.0×10^5	1.0×10^4	2.0×10^4	
MDR [e]	-	0.7 to 2×10^7	1.4×10^8	8×10^7	Carey and Sigurdsson (1987)
$D_{conduit}$ [f]	-	35-40 m (43)	50 m (51)	65 m	Mastin and Ghiorso (2000), Neri et al. (2002)
$D_{conduit}$ [g]	4 m	30-36 m	42 m	62 m	Cioni, unpublished data.
V_{exit} [h]	-	160 m s^{-1} (185)	141 m s^{-1} (156)	150 m s^{-1}	Mastin and Ghiorso (2000), Neri et al. (2002)
H_2O [h]	4.5-6 wt%	4.5-6 wt%	2.7-3.5 wt%	2.7-3.5 wt%	Cioni et al. (1995), Cioni (2000), Larsen (2008)
SiO_2	54.91 (0.26)	55.41 (0.38)	54.73 (0.48)	54.88 (0.34)	Cioni et al. (1995)
TiO_2	0.31 (0.14)	0.26 (0.11)	0.54 (0.05	0.56 (0.03	Larsen (2008)
Al_2O_3	22.30 (0.23)	21.97 (0.45)	19.36 (024)	18.57 (0.46)	Shea et al. (2009)
FeO*	2.16 (0.13)	2.90 (0.38)	4.60 (0.33)	4.81 (0.26)	
MnO	0.24 (0.08)	0.24 (0.12)	0.14 (0.01)	0.13 (0.01)	
MgO	0.23 (0.03)	0.65 (0.07)	1.60 (0.31)	2.31 (0.41)	
CaO	3.11 (0.22)	3.69 (0.25)	5.35 (0.30)	5.87 (0.63)	
Na_2O	6.22 (0.19)	5.32 (0.21)	4.49 (0.29)	4.26 (0.42)	
K_2O	9.89 (0.42)	9.17 (0.39)	9.04 (0.14)	8.37 (0.64)	
P_2O_5	0.09 (0.04)	0.12 (0.05)	0.18 (0.03)	0.23 (0.03)	

a. Vesicle-free magma density obtained by He-pycnometry on powdered samples (Shea et al. in prep).
b. Magma temperature
c. Total crystal content (microphenocrysts+phenocrysts)
d. Magma viscosity (μ_{m+c} is viscosity of melt+crystals, μ_{m+c+b} [1] is viscosity of melt+crystals+bubbles assuming bubbles have Ca<1, μ_{m+c+b} [2] is viscosity of melt+crystals+bubbles assuming bubbles have Ca>>1). Calculations were performed for pressures of 100 MPa at lower conduit conditions and at 15 MPa, near fragmentation level.
e. Mass discharge rates from Carey and Sigurdsson (1987)
f. Values of conduit diameter computed using Conflow (Mastin, 2005). Back-simulations were performed to best match the output MDR to the values of Carey and Sigurdsson (1987), using input values from the table above (i.e. composition, water content, temperature, and an initial pressure of 100 MPa). Because Conflow models deal less well with highly crystalline mixtures, the obtained values for EU3top are subject to more uncertainty.

Values of conduit radius calculated by Neri et al. (2002) for the 79AD eruption are also shown in parentheses for comparison.

g. Values of conduit diameter calculated by integrating over the entire fallout units the mass of deep carbonate wallrock (% abundance × deposit thickness × deposit density) over 24 sampling sites, from 5 to 90 km from the vent.
h. Exit velocity obtained from the Conflow simulations with values from Neri et al. (2002) in parentheses.
i. Dissolved water contents, and major oxide analyses normalized to 100 wt% (dry).
j. Deposits EU3base and EU3 max are lumped together since their chemistry/crystal content are about the same.